

Optimal polarized observables for model-independent new-physics search at e^+e^- colliders

A.A. Babich^a, P. Osland^b, A.A. Pankov^{a,c}, and N. Paver^c

^a Pavel Sukhoi Technical University, Gomel, 246746 Belarus

^b Department of Physics, University of Bergen,
Allégaten 55, N-5007 Bergen, Norway

^c Dipartimento di Fisica Teorica, Università di Trieste and
Istituto Nazionale di Fisica Nucleare, Sezione di Trieste, Trieste, Italy

Abstract

For the processes $e^+e^- \rightarrow \mu^+\mu^-$, $\tau^+\tau^-$, $b\bar{b}$ and $c\bar{c}$ at a future e^+e^- collider with $\sqrt{s} = 0.5$ TeV, we examine the sensitivity of the helicity cross sections to four-fermion contact interactions. If longitudinal polarization of the electron beam were available, two polarized integrated cross sections would offer the opportunity to separate the helicity cross sections and, in this way, to derive model-independent bounds on the relevant parameters. The measurement of these polarized cross sections with optimal kinematical cuts could significantly increase the sensitivity of helicity cross sections to contact interaction parameters and could give crucial information on the chiral structure of such new interactions.

1 Introduction

Any measured deviation from the Standard Model (SM) predictions in electron-positron annihilation into fermion-pairs

$$e^+ + e^- \rightarrow f + \bar{f} \quad (1)$$

($f = l$ or q for lepton or quark) would signal the presence of new phenomena. By means of the effective Lagrangian approach, four-fermion contact interactions offer a general framework for describing low-energy manifestations of non-standard interactions active at a very high energy scale Λ , which in many cases can be interpreted as the mass of a new heavy particle exchanged in the process, with a strength governed by some effective coupling constant g_{eff} [1, 2].

At sub-TeV energies, representative examples are the exchange of a Z' with a few TeV mass and the exchange of a heavy leptoquark. In general, any new interaction generated by s , t or u exchanges of objects with mass-squared much larger than the corresponding Mandelstam variables can be described by effective four-fermion $eeff$ local interactions [3, 4]. This is also the case, in the context of supersymmetry, of R -parity breaking interactions at energies much smaller than the sparticle masses, and of the composite models of quarks and leptons, where contact interactions arise as a remnant of the binding force between the fermion substructure constituents.

Thus, the concept of contact interactions with a universal energy scale Λ is quite generally used, also in other processes besides (1) such as ep and $p\bar{p}$ collisions, to conveniently parameterize deviations from the SM that may be caused by some new physics at the large energy scale Λ .

The lowest-order four-fermion contact terms have dimension $D = 6$, which implies that they are suppressed by $g_{\text{eff}}^2/\Lambda^2$. Restricting the fermion currents to be helicity conserving and flavor diagonal, the general $SU(3) \times SU(2) \times U(1)$ invariant four-fermion $eeff$ contact interaction Lagrangian with $D = 6$ can be written as [1–4]:

$$\begin{aligned} \mathcal{L} = \frac{g_{\text{eff}}^2}{\Lambda^2} & \left[\eta_{\text{LL}} (\bar{e}_L \gamma_\mu e_L) (\bar{f}_L \gamma^\mu f_L) + \eta_{\text{LR}} (\bar{e}_L \gamma_\mu e_L) (\bar{f}_R \gamma^\mu f_R) \right. \\ & \left. + \eta_{\text{RL}} (\bar{e}_R \gamma_\mu e_R) (\bar{f}_L \gamma^\mu f_L) + \eta_{\text{RR}} (\bar{e}_R \gamma_\mu e_R) (\bar{f}_R \gamma^\mu f_R) \right], \end{aligned} \quad (2)$$

where generation and color indices have been suppressed.¹ The subscripts L and R indicate that the current in each parenthesis can be either left- or right-handed, and the parameters $\eta_{\alpha\beta}$ ($\alpha, \beta = \text{L, R}$) determine the chiral structure of the interaction. Although in a purely phenomenological approach they are free parameters, conventionally they are taken to be $\eta_{\alpha\beta} = \pm 1$ or 0. Also, it is conventional to take $g_{\text{eff}}^2 = 4\pi$, as reminiscence of the fact that such contact interactions were initially introduced in the framework of compositeness, where the new binding forces were assumed to be strong.

In general, for a given fermion flavor f , Eq. (2) defines eight independent, individual interaction models corresponding to the combinations of the four chiralities LL, LR, RL and

¹For the case of $t\bar{t}$ final states, see [5].

RR with the \pm signs of the η 's. In practice, the true interaction might correspond to one of these models or to any combination of them. The number of independent coefficients could be reduced by imposing symmetries that provide relations among the contact interaction couplings [4].² Here, we will not consider any particular symmetry. We will instead perform a model-independent analysis considering contact interaction couplings of magnitude $\eta_{\alpha\beta} = \pm 1$, and independent mass-scales $\Lambda_{\alpha\beta}$ corresponding to each of the helicity combinations in Eq. (2). For our purpose of obtaining constraints on the $\Lambda_{\alpha\beta}$, the signs of the η 's turn out to be numerically unimportant. Indeed, for given helicities $\alpha\beta$, different signs η yield practically identical results for the mass scales $\Lambda_{\alpha\beta}$ because, in the chosen kinematical configuration, the non-standard effects are largely dominated by the interference between the contact interaction and the SM terms.

Clearly, the definition of Λ adopted here, provides a standard for comparing the power of different new-physics searches. For example, a bound on Λ would mean that a Z' with couplings of the order of the electromagnetic couplings could exist with mass down to $M_{Z'} \sim \sqrt{\alpha} \Lambda$, and the same would be true for leptoquarks and for any new, very heavy gauge bosons that may be exchanged in the process under consideration.

In principle, the sought-for deviations of observables from the SM predictions, giving information on Λ 's, simultaneously depend on all four-fermion effective coupling constants in Eq. (2), which therefore cannot be easily disentangled. For simplicity, the analysis is usually performed by taking a non-zero value for only one parameter at a time, all the remaining ones being put equal to zero. Limits on individual $eeqq$ contact interaction parameters have recently been derived by this procedure, from a global analysis of the relevant data [4], and the individual models are severely constrained, with $\Lambda_{\alpha\beta} \sim \mathcal{O}(10)$ TeV.

However, if several terms of different chiralities were simultaneously taken into account, cancellations may occur and the resulting bounds on $\Lambda_{\alpha\beta}$ would be considerably weaker, of the order of 3 – 4 TeV. As an example, the constraints originating from atomic parity violation experiments could be substantially relaxed if there were compensating contributions from different terms [6]. Consequently, a definite improvement of the situation in this regard should be obtained from a procedure of analyzing experimental data that allows to account for the various contact interaction couplings simultaneously as free parameters, and yet to obtain in a model-independent way separate bounds for the corresponding Λ 's, not affected by possible accidental cancellations.

For that purpose, we propose an analysis of $eell$, $eebb$ and $eecc$ contact interactions at the next linear e^+e^- collider (LC) with $\sqrt{s} = 500$ GeV and with longitudinally polarized beams. Our approach makes use of two particular, polarized, integrated cross sections σ_1 and σ_2 (see Eqs. (21) and (22)), that are directly connected, *via* linear combinations, to the helicity cross sections of process (1), and therefore allow to deal with a minimal set of independent free parameters.

This kind of observables, defined for specific kinematical cuts, were already introduced to study Z' signals at LEP2 and LC [7, 8] and potential manifestations of compositeness at

²For example, for Z' exchange, $\eta_{LL}\eta_{RR} = \eta_{LR}\eta_{RL}$.

the LC [9]. Here, we extend the previous considerations by performing a general analysis where, in the definition of the above-mentioned integrated observables, we choose suitable kinematical regions where the sensitivity to individual four-fermion contact interaction parameters is maximal. As we shall see, this procedure of optimization results in a further increase of sensitivity, that for some of the four-fermion interactions can be quite substantial. Moreover, we make a short comparison of the numerical bounds on Λ 's with the results of the more commonly used observables.

2 Polarized observables

In the Born approximation, including the γ and Z exchanges as well as the four-fermion contact interaction term (2), but neglecting m_f with respect to the c.m. energy \sqrt{s} , the differential cross section for the process $e^+e^- \rightarrow f\bar{f}$ ($f \neq e, t$) with longitudinally polarized electron-positron beams, can be written as [10]

$$\frac{d\sigma}{d\cos\theta} = \frac{3}{8} [(1 + \cos\theta)^2 \sigma_+ + (1 - \cos\theta)^2 \sigma_-], \quad (3)$$

where θ is the angle between the incoming electron and the outgoing fermion in the c.m. frame. The functions σ_{\pm} can be expressed in terms of helicity cross sections

$$\sigma_{\alpha\beta} = N_C \sigma_{\text{pt}} |A_{\alpha\beta}|^2, \quad (4)$$

with $\alpha, \beta = \text{L, R}$. Here, N_C is the QCD factor: $N_C \approx 3(1 + \alpha_s/\pi)$ for quarks and $N_C = 1$ for leptons, respectively, and $\sigma_{\text{pt}} \equiv \sigma(e^+e^- \rightarrow \gamma^* \rightarrow l^+l^-) = (4\pi\alpha^2)/(3s)$. With electron and positron longitudinal polarizations P_e and $P_{\bar{e}}$, the relations are

$$\sigma_+ = \frac{1}{4} [(1 - P_e)(1 + P_{\bar{e}}) \sigma_{\text{LL}} + (1 + P_e)(1 - P_{\bar{e}}) \sigma_{\text{RR}}], \quad (5)$$

$$\sigma_- = \frac{1}{4} [(1 - P_e)(1 + P_{\bar{e}}) \sigma_{\text{LR}} + (1 + P_e)(1 - P_{\bar{e}}) \sigma_{\text{RL}}]. \quad (6)$$

The helicity amplitudes $A_{\alpha\beta}$ can be written as

$$A_{\alpha\beta} = Q_e Q_f + g_{\alpha}^e g_{\beta}^f \chi_Z + \frac{s\eta_{\alpha\beta}}{\alpha\Lambda_{\alpha\beta}^2}, \quad (7)$$

where the gauge boson propagator is $\chi_Z = s/(s - M_Z^2 + iM_Z\Gamma_Z)$, the SM left- and right-handed fermion couplings of the Z are $g_L^f = (I_{3L}^f - Q_f s_W^2)/s_W c_W$ and $g_R^f = -Q_f s_W^2/s_W c_W$ with $s_W^2 = 1 - c_W^2 \equiv \sin^2 \theta_W$, and Q_f are the fermion electric charges.

The total cross section and the difference of forward and backward cross sections are given as

$$\begin{aligned} \sigma &= \sigma_+ + \sigma_- = \frac{1}{4} [(1 - P_e)(1 + P_{\bar{e}})(\sigma_{\text{LL}} + \sigma_{\text{LR}}) + (1 + P_e)(1 - P_{\bar{e}})(\sigma_{\text{RR}} + \sigma_{\text{RL}})], \quad (8) \\ \sigma_{\text{FB}} &\equiv \sigma_{\text{F}} - \sigma_{\text{B}} = \frac{3}{4} (\sigma_+ - \sigma_-) \\ &= \frac{3}{16} [(1 - P_e)(1 + P_{\bar{e}})(\sigma_{\text{LL}} - \sigma_{\text{LR}}) + (1 + P_e)(1 - P_{\bar{e}})(\sigma_{\text{RR}} - \sigma_{\text{RL}})], \quad (9) \end{aligned}$$

where

$$\sigma_F = \int_0^1 (d\sigma/d \cos \theta) d \cos \theta, \quad \sigma_B = \int_{-1}^0 (d\sigma/d \cos \theta) d \cos \theta. \quad (10)$$

Taking Eq. (7) into account, these relations show that in general σ and σ_{FB} simultaneously involve all contact-interactions couplings even in the polarized case. Therefore, by themselves, these measurements do not allow a completely model-independent analysis avoiding, in particular, potential cancellations among different couplings.

Our analysis will be based on the consideration of the four helicity cross sections $\sigma_{\alpha\beta}$ as the basic independent observables to be measured from data on the polarized differential cross section. These cross sections depend each on just one individual four-fermion contact parameter and therefore lead to a model-independent analysis where all $\eta_{\alpha\beta}$ can be taken simultaneously into account as completely free parameters, with no danger from potential cancellations. As Eqs. (5) and (6) show, helicity cross sections can be disentangled *via* the measurement of σ_+ and σ_- with different choices of the initial beam polarizations.

One possibility is to project out σ_+ and σ_- from $d\sigma/d \cos \theta$, as differences of integrated cross sections. To this aim, we define $z_{\pm}^* \equiv \cos \theta_{\pm}^*$ such that

$$\left(\int_{z_{\pm}^*}^1 - \int_{-1}^{z_{\pm}^*} \right) (1 \mp \cos \theta)^2 d \cos \theta = 0. \quad (11)$$

One finds the solutions: $z_{\pm}^* = \mp(2^{2/3} - 1) = \mp 0.587$ ($\theta_+^* = 126^\circ$ and $\theta_-^* = 54^\circ$).³

From Eq. (3) one can easily see that at these values of z_{\pm}^* the difference of two integrated cross sections defined as

$$\sigma_1(z_{\pm}^*) - \sigma_2(z_{\pm}^*) \equiv \left(\int_{z_{\pm}^*}^1 - \int_{-1}^{z_{\pm}^*} \right) \frac{d\sigma}{d \cos \theta} d \cos \theta \quad (12)$$

is directly related to σ_{\pm} as:

$$\sigma_1(z_+^*) - \sigma_2(z_+^*) = \gamma \sigma_+, \quad \sigma_2(z_-^*) - \sigma_1(z_-^*) = \gamma \sigma_-, \quad (13)$$

where $\gamma = 3(2^{2/3} - 2^{1/3}) = 0.982$.

The solutions of the system of two equations corresponding to $P_e = \pm P$, and assuming unpolarized positrons $P_{\bar{e}} = 0$, in Eqs. (5) and (6), can be written as:

$$\sigma_{LL} = \frac{1+P}{P} \sigma_+(-P) - \frac{1-P}{P} \sigma_+(P), \quad (14)$$

$$\sigma_{RR} = \frac{1+P}{P} \sigma_+(P) - \frac{1-P}{P} \sigma_+(-P), \quad (15)$$

$$\sigma_{LR} = \frac{1+P}{P} \sigma_-(-P) - \frac{1-P}{P} \sigma_-(P), \quad (16)$$

$$\sigma_{RL} = \frac{1+P}{P} \sigma_-(P) - \frac{1-P}{P} \sigma_-(-P). \quad (17)$$

³These values satisfy $(z_{\pm}^* \mp 1)^3 = \mp 4$. In the case of $|\cos \theta| = c < 1$, one has $|z_{\pm}^*| = (1 + 3c^2)^{1/3} - 1$.

From Eqs. (14)–(17) one can easily see that this procedure allows to extract σ_{LL} , σ_{RR} , σ_{LR} and σ_{RL} by the four independent measurements of $\sigma_1(z_\pm^*)$ and $\sigma_2(z_\pm^*)$ at $P_e = \pm P$.

The kind of analysis given above shows that the separation of the helicity cross sections can be performed by means of two independent integrated observables (i.e., cross sections) at two different values of polarization.⁴ Clearly, the measurement of four independent observables is a minimum to perform such separations.

In the sequel, we shall make a comparison of the sensitivity to contact-interaction couplings of the helicity cross sections determined by the procedure outlined above, and the corresponding discovery limits on $\Lambda_{\alpha\beta}$, to the results of an analysis based on a χ^2 fit to the set of ‘conventional’ observables represented by $\sigma(P = 0)$, the forward-backward asymmetry (also for $P = 0$)

$$A_{FB} = \frac{\sigma_{FB}}{\sigma}, \quad (18)$$

the left-right asymmetry

$$A_{LR} = \frac{\sigma_L - \sigma_R}{\sigma_L + \sigma_R} = \frac{\sigma_{LL} - \sigma_{RR} + \sigma_{LR} - \sigma_{RL}}{\sigma_{LL} + \sigma_{RR} + \sigma_{LR} + \sigma_{RL}}, \quad (19)$$

and the combined left-right forward-backward asymmetry

$$A_{LR,FB} = \frac{(\sigma_L^F - \sigma_R^F) - (\sigma_L^B - \sigma_R^B)}{(\sigma_L^F + \sigma_R^F) + (\sigma_L^B + \sigma_R^B)} = \frac{3}{4} \frac{\sigma_{LL} - \sigma_{RR} + \sigma_{RL} - \sigma_{LR}}{\sigma_{LL} + \sigma_{RR} + \sigma_{RL} + \sigma_{LR}}, \quad (20)$$

where σ_L and σ_R denote the cross sections with left-handed and right-handed electrons and unpolarized positrons.

3 Generalization and radiative corrections

This extraction of helicity cross sections can be obtained more generally. Indeed, let us divide the full angular range, $|\cos \theta| \leq 1$ into two parts, $(-1, z^*)$ and $(z^*, 1)$, with arbitrary z^* , and define two integrated cross sections as

$$\sigma_1(z^*) \equiv \int_{z^*}^1 \frac{d\sigma}{d\cos\theta} d\cos\theta = \frac{1}{8} \{ [8 - (1 + z^*)^3] \sigma_+ + (1 - z^*)^3 \sigma_- \}, \quad (21)$$

$$\sigma_2(z^*) \equiv \int_{-1}^{z^*} \frac{d\sigma}{d\cos\theta} d\cos\theta = \frac{1}{8} \{ (1 + z^*)^3 \sigma_+ + [8 - (1 - z^*)^3] \sigma_- \}. \quad (22)$$

Solving these two equations, one finds the general relations

$$\sigma_+ = \frac{1}{6(1 - z^{*2})} [(8 - (1 - z^*)^3) \sigma_1(z^*) - (1 - z^*)^3 \sigma_2(z^*)], \quad (23)$$

$$\sigma_- = \frac{1}{6(1 - z^{*2})} [-(1 + z^*)^3 \sigma_1(z^*) + (8 - (1 + z^*)^3) \sigma_2(z^*)], \quad (24)$$

⁴An alternative possibility to disentangle the helicity cross sections in the process (1) based on differential distributions was studied in [11]. However, with limited statistics, the approach exploiting integrated observables has an advantage.

that allow to disentangle the helicity cross sections, using (14)–(17) and the availability of polarized beams.

In order to extract the helicity cross sections, we thus make use of *two* sets of integrated cross sections. The basic ones are $\sigma_1(z^*, P)$ and $\sigma_2(z^*, P)$, which depend both on the kinematical cut z^* and the polarization. From these, as a second step, we construct the cross sections $\sigma_+(P)$ and $\sigma_-(P)$ of the previous section, which finally yield the helicity cross sections $\sigma_{\alpha\beta}$.

It is instructive to consider some particular cases depending on the choice of z^* :

- (i) If one chooses $z^* = 0$, then $\sigma_{1,2} = \sigma_{\text{F,B}}$ and, from (23) and (24), $(7\sigma_{\text{F,B}} - \sigma_{\text{B,F}})/6 = \sigma_{\pm}$.
- (ii) Requiring $z^* = z_+^* = 1 - 2^{2/3} = -0.587$, one re-obtains the first relation in Eq. (13) and $(1 - \gamma^{-1})\sigma_1 + (1 + \gamma^{-1})\sigma_2 = \sigma_-$.
- (iii) Taking $z^* = z_-^* = -1 + 2^{2/3} = 0.587$, one re-obtains the second relation in Eq. (13) and $(1 + \gamma^{-1})\sigma_1 + (1 - \gamma^{-1})\sigma_2 = \sigma_+$.
- (iv) For unpolarized initial beams ($P = 0$), which is the case at LEP2, only linear combinations of helicity cross sections can be separated:

$$\frac{1}{4}(\sigma_{\text{LL}} + \sigma_{\text{RR}}) = \sigma_+, \quad \frac{1}{4}(\sigma_{\text{LR}} + \sigma_{\text{RL}}) = \sigma_-. \quad (25)$$

The previous formulae continue to hold, with the inclusion of one-loop SM electroweak radiative corrections, in the form of improved Born amplitudes. Basically, the parameterization that uses the best known SM parameters G_{F} , M_Z and $\alpha(M_Z^2)$ is obtained by replacing $\alpha \Rightarrow \alpha(M_Z^2)$ and $\sin^2 \theta_W \Rightarrow \sin^2 \theta_W^{\text{eff}}$ in the above equations and [12, 13]:

$$g_{\text{L}}^f \Rightarrow \frac{2}{\sqrt{\kappa}} \left(I_{3\text{L}}^f - Q_f \sin^2 \theta_W^{\text{eff}} \right), \quad g_{\text{R}}^f \Rightarrow -\frac{2Q_f}{\sqrt{\kappa}} \sin^2 \theta_W^{\text{eff}}, \quad \sin^2(2\theta_W^{\text{eff}}) \equiv \kappa = \frac{4\pi\alpha(M_Z^2)}{\sqrt{2}G_{\text{F}}M_Z^2\rho}, \quad (26)$$

with $\rho \approx 1 + 3G_{\text{F}}m_{\text{top}}^2/(8\pi^2\sqrt{2})$. Moreover, for the Z -propagator: $\chi_Z(s) \Rightarrow s/(s - M_Z^2 + i(s/M_Z^2)M_Z\Gamma_Z)$.

We take radiative corrections into account by means of the program ZFITTER [14], which has to be used along with ZEFIT, adapted to the present discussion. We thus include initial- and final-state radiation, and the interference between them. Initial state radiation (ISR) is of major importance for contact interaction searches. The observed cross section is significantly distorted in shape and magnitude by the emission of real photons by the incoming electrons and positrons [15]. In the mentioned program, the hard photon radiation is calculated up to order α^2 and the leading soft and virtual corrections are summed to all orders by the exponentiation technique. The final expression for the differential cross section is of the same form as Eq. (3), where the scattering angle refers to that between the final-state fermion f and the e^- beam direction in the $f\bar{f}$ centre-of-mass system [16]. The symmetric and antisymmetric parts of the cross section, $\sigma_{s,a}$, are given by convolutions with the ‘radiators’:

$$\sigma_s = \int_0^\Delta dk R_{\text{T}}^e(k) \sigma(s'), \quad \sigma_a = \frac{4}{3} \int_0^\Delta dk R_{\text{FB}}^e(k) \sigma_{\text{FB}}(s'), \quad (27)$$

with $s' = s(1 - k)$, and $k = E_\gamma/E_{\text{beam}}$ the fraction of energy lost by radiation, and $R_T^e(k)$ and $R_{\text{FB}}^e(k)$ the radiator functions, whose explicit expression can be found in ref. [14].

Due to the radiative return to the Z resonance at $\sqrt{s} > M_Z$, the energy spectrum of the radiated photons is peaked around $k_{\text{peak}} \approx 1 - M_Z^2/s$ [15]. In order to increase the signal originating from contact interactions, events with hard photons should be eliminated by an appropriate cut $\Delta < k_{\text{peak}}$ on the photon energy. Since the form of the corrected cross section is the same as that of Eq. (3), it follows that the radiatively-corrected $\sigma_{1,2}$ can also be defined by Eqs. (21) and (22), with the same value for z^* . For our numerical analysis, we use $m_{\text{top}} = 175$ GeV, $m_H = 100$ GeV and a cut $\sqrt{s'} \geq 0.9\sqrt{s}$ to avoid the radiative return to the Z peak for $\sqrt{s} = 0.5$ TeV.

The convenience of $\sigma_{1,2}$ of Eqs. (21) and (22) as experimental integrated observables will be appreciated in the next Section, where the numerical analysis and the corresponding bounds on Λ 's will be 'optimized' by suitable choices of the z^* values that maximize the sensitivity to such non-standard interactions.

4 Sensitivity and optimization

In the case where no deviation from the SM is observed, one can make an assessment of the sensitivity of the process (1) to the contact interaction parameters, based on the expected experimental accuracy on the observables $\sigma_{\alpha\beta}$. Such sensitivity numerically determines the bounds on the contact-interaction scales $\Lambda_{\alpha\beta}$ that can be derived from the experimental data and, basically, is determined by the comparison of deviations from the SM predictions due to the contact-interaction terms with the attainable experimental uncertainty. Accordingly, we define the 'significance' of each helicity cross section by the ratio:

$$\mathcal{S} = \frac{|\Delta\sigma_{\alpha\beta}|}{\delta\sigma_{\alpha\beta}}, \quad (28)$$

where $\Delta\sigma_{\alpha\beta}$ is the deviation from the SM prediction, dominated for $\sqrt{s} \ll \Lambda_{\alpha\beta}$ by the interference term:

$$\Delta\sigma_{\alpha\beta} \equiv \sigma_{\alpha\beta} - \sigma_{\alpha\beta}^{\text{SM}} \simeq 2N_C \sigma_{\text{pt}} \left(Q_e Q_f + g_\alpha^e g_\beta^f \chi_Z \right) \frac{s\eta_{\alpha\beta}}{\alpha\Lambda_{\alpha\beta}^2}, \quad (29)$$

and $\delta\sigma_{\alpha\beta}$ is the expected experimental uncertainty on $\sigma_{\alpha\beta}$, combining statistical and systematic uncertainties.

For example, adding uncertainties in quadrature, the uncertainty on σ_{LL} , indirectly measured *via* σ_1 and σ_2 (see Eqs. (14) and (23)), is given by

$$\begin{aligned} (\delta\sigma_{LL})^2 &= a^2(z^*) \left(\frac{1+P}{P} \right)^2 (\delta\sigma_1(z^*, -P))^2 + a^2(z^*) \left(\frac{1-P}{P} \right)^2 (\delta\sigma_1(z^*, P))^2 \\ &\quad + b^2(z^*) \left(\frac{1+P}{P} \right)^2 (\delta\sigma_2(z^*, -P))^2 + b^2(z^*) \left(\frac{1-P}{P} \right)^2 (\delta\sigma_2(z^*, P))^2, \end{aligned} \quad (30)$$

where

$$a(z^*) = \frac{8 - (1 - z^*)^3}{6(1 - z^{*2})}, \quad b(z^*) = -\frac{(1 - z^*)^3}{6(1 - z^{*2})}. \quad (31)$$

Analogous expressions hold for the combinations related to the uncertainties $\delta\sigma_{\text{RR}}$, $\delta\sigma_{\text{LR}}$ and $\delta\sigma_{\text{RL}}$. Numerically, in the situation of small deviations from the SM we are considering, we can use to a very good approximation the SM predictions for the cross sections $\sigma_{1,2}$ to assess the expected $\delta\sigma_{1,2}$ and therefore of the uncertainties $\delta\sigma_{\alpha\beta}$ in the denominator of (28). Basically, the directly measured integrated cross sections $\sigma_{1,2}$ of Eqs. (21) and (22) and, correspondingly, the uncertainties $\delta\sigma_{\alpha\beta}$, are dependent on the value of z^* , which can be considered in general as an input parameter related to given experimental conditions (see, *e.g.*, Eq. (30)). Since the deviation $\Delta\sigma_{\alpha\beta}$ of Eq. (29) is independent of z^* , the full sensitivity of a given helicity cross section to the relevant contact-interaction parameter is determined by the corresponding size and z^* behavior of the uncertainty $\delta\sigma_{\alpha\beta}$. Then, the optimization would be obtained by choosing for z^* the value z_{opt}^* where the uncertainty $\delta\sigma_{\alpha\beta}$ becomes minimum, *i.e.*, where the corresponding sensitivity Eq. (28) has a maximum. As anticipated, we estimate the required z^* behavior from the known SM cross sections.

Accordingly, statistical uncertainties will be given by

$$(\delta\sigma_i)_{\text{stat}}^2 \simeq (\delta\sigma_i^{\text{SM}})_{\text{stat}}^2 = \frac{\sigma_i^{\text{SM}}}{\epsilon \mathcal{L}_{\text{int}}}, \quad i = 1, 2, \quad (32)$$

where \mathcal{L}_{int} is the integrated luminosity, and ϵ is the efficiency for detecting the final state under consideration. The equation that determines the values of z^* that minimize the statistical uncertainties on $\sigma_{\alpha\beta}$ is:

$$z^* = -3 \frac{1 - r_{\alpha\beta}}{1 + r_{\alpha\beta}} \frac{z^{*4} - 6z^{*2} - 3}{z^{*4} - 2z^{*2} - 23}, \quad (33)$$

where

$$r_{\text{LL}} = r_{\text{LR}} = \frac{(1 + 3P^2)\sigma_{\text{LR}}^{\text{SM}} + (1 - P^2)\sigma_{\text{RL}}^{\text{SM}}}{(1 + 3P^2)\sigma_{\text{LL}}^{\text{SM}} + (1 - P^2)\sigma_{\text{RR}}^{\text{SM}}}, \quad (34)$$

and $r_{\text{RR}} = r_{\text{RL}}$ is obtained by replacing $\text{L} \leftrightarrow \text{R}$ in (34). As one can see, the location of z^* that minimizes the statistical uncertainty, only depends on the SM parameters and P , and is independent from the luminosity and efficiency of reconstruction ϵ of a final-state fermion. In a left-right symmetric theory, the above ratios $r_{\alpha\beta}$ would all be 1, and in this case $z^* = 0$. However, in the SM, depending on flavour and energy, $r_{\alpha\beta}$ may be less than, or larger than unity. Since the z^* -dependent fraction in (33) is positive for $z^{*2} \leq 1$, it follows that the solutions satisfy $z^* < 0$ if $r_{\alpha\beta} < 1$ and *vice versa*. We also note that the location is the same for the LL and LR configurations, and likewise for RR and RL, while numerically the sensitivities are different. The numerical solutions of Eq. (33) are reported in Table 1 for different values of longitudinal polarization of electrons P .

process	P	$r_{LL}; r_{LR}$	z_{opt}^*	$r_{RR}; r_{RL}$	z_{opt}^*
$e^+e^- \rightarrow l^+l^-$	1.0	0.19	-0.32	0.24	-0.28
	0.9	0.19	-0.32	0.23	-0.28
	0.5	0.20	-0.30	0.22	-0.29
$e^+e^- \rightarrow b\bar{b}$	1.0	0.06	-0.51	0.30	-0.23
	0.9	0.07	-0.50	0.24	-0.27
	0.5	0.08	-0.47	0.13	-0.32
$e^+e^- \rightarrow c\bar{c}$	1.0	0.14	-0.38	0.07	-0.48
	0.9	0.13	-0.38	0.08	-0.47
	0.5	0.12	-0.39	0.10	-0.46

Table 1: Optimal values of z_{opt}^* obtained from Eq. (33) at $E_{\text{c.m.}} = 0.5$ TeV.

Clearly, the optimal values of z^* reported in Table 1 can be applied in practice in the case of low statistics, where the statistical uncertainty dominates over the systematic one. In the general case, the latter can affect the determination of the value of z_{opt}^* , especially in the case of higher luminosity, where it may dominate over the statistical uncertainties. Combining, again in quadrature, statistical and systematic uncertainties on $\sigma_{1,2}$, we have:

$$(\delta\sigma_i)^2 \simeq (\delta\sigma_i^{\text{SM}})^2 = \frac{\sigma_i^{\text{SM}}}{\epsilon \mathcal{L}_{\text{int}}} + (\delta^{\text{sys}} \sigma_i^{\text{SM}})^2. \quad (35)$$

Numerically, for $\sigma_{1,2}$ we take into account the expected identification efficiencies, ϵ [18] and the systematic uncertainties, δ^{sys} , on the various fermionic final states, for which we assume: for leptons: $\epsilon = 95\%$ and $\delta^{\text{sys}} = 0.5\%$; for b quarks: $\epsilon = 60\%$ and $\delta^{\text{sys}} = 1\%$; for c quarks: $\epsilon = 35\%$ and $\delta^{\text{sys}} = 1.5\%$. As concerns the systematic uncertainty, we assume the same δ^{sys} for $i = 1, 2$, and independent of z^* in the relevant angular range.

We consider the LC with the following options: $\sqrt{s} = 0.5$ TeV, $\mathcal{L}_{\text{int}} = 50 \text{ fb}^{-1}$ up to $\mathcal{L}_{\text{int}} = 500 \text{ fb}^{-1}$ to assess the role of statistics, $P = 0.9$ and $|\cos\theta| \leq 0.99$. We assume half the total integrated luminosity quoted above for both values of the electron polarization, $P_e = \pm P$.

The relative uncertainties, $\delta\sigma_{\alpha\beta}/\sigma_{\alpha\beta}$, on the helicity cross sections, are shown as functions of z^* in Figs. 1,2 for different final states. The optimal kinematical parameters z_{opt}^* where the sensitivity is a maximum, can easily be obtained from these figures. Inclusion of systematic errors results in changing the location of z_{opt}^* such that it increases for the cases of LL and RR helicity configurations and decreases for LR and RL. When the two intervals are very different, $z^* \rightarrow \pm 1$, the uncertainty blows up like $1/\sqrt{1 \mp z^*}$, because the corresponding cross section σ_1 or σ_2 vanishes with $1 \mp z^*$, respectively. Since, in these figures, the lowest value for \mathcal{L}_{int} is considered, the optimal values of z^* are close to those in Table 1, because the statistical uncertainty dominates in the considered situation. In Table 2, we report the behaviour of z_{opt}^* with luminosity.

In order to assess the increase of sensitivity obtained by optimization, one should compare the corresponding uncertainties at z_{opt}^* with those obtained without optimization, at

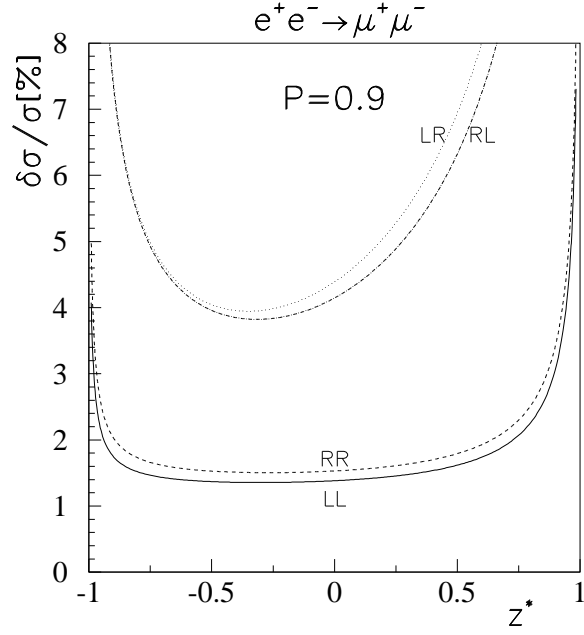


Figure 1: The uncertainty on the helicity cross sections $\sigma_{\alpha\beta}$ in the SM as a function of z^* for the process $e^+e^- \rightarrow \mu^+\mu^-$ at $\sqrt{s} = 0.5$ TeV, $\mathcal{L}_{\text{int}} = 50 \text{ fb}^{-1}$, $P = 0.9$, $\epsilon = 95\%$ and $\delta^{\text{sys}} = 0.5\%$. Radiative corrections are included.

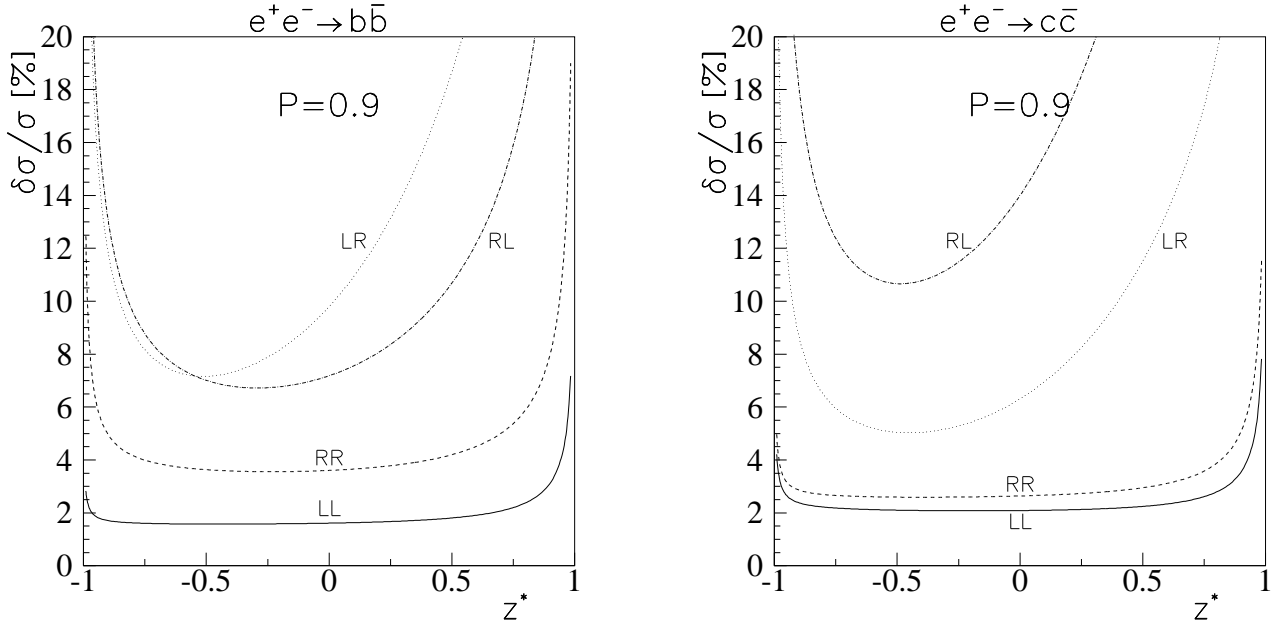


Figure 2: Same as in Fig. 1, but for the processes $e^+e^- \rightarrow b\bar{b}$ at $\epsilon = 60\%$ and $\delta^{\text{sys}} = 1.0\%$, and $e^+e^- \rightarrow c\bar{c}$ at $\epsilon = 35\%$ and $\delta^{\text{sys}} = 1.5\%$.

\mathcal{L}_{int} fb $^{-1}$	z_{LL}^*			z_{RR}^*			z_{LR}^*			z_{RL}^*		
	l^+l^-	$b\bar{b}$	$c\bar{c}$	l^+l^-	$b\bar{b}$	$c\bar{c}$	l^+l^-	$b\bar{b}$	$c\bar{c}$	l^+l^-	$b\bar{b}$	$c\bar{c}$
50	-0.30	-0.45	-0.19	-0.27	-0.23	-0.39	-0.35	-0.51	-0.45	-0.32	-0.29	-0.49
100	-0.28	-0.37	-0.09	-0.24	-0.20	-0.34	-0.36	-0.53	-0.50	-0.33	-0.31	-0.51
200	-0.22	-0.33	0.13	-0.19	-0.14	-0.23	-0.39	-0.56	-0.55	-0.35	-0.34	-0.54
300	-0.17	-0.25	0.28	-0.13	-0.08	-0.11	-0.41	-0.58	-0.58	-0.37	-0.37	-0.56
400	-0.11	-0.17	0.35	-0.09	-0.03	-0.00	-0.43	-0.59	-0.60	-0.40	-0.39	-0.58
500	-0.07	-0.03	0.41	-0.05	-0.01	0.11	-0.44	-0.61	-0.62	-0.41	-0.40	-0.59

Table 2: z_{opt}^* vs. \mathcal{L}_{int} for the processes $e^+e^- \rightarrow \mu^+\mu^-$; $b\bar{b}$; $c\bar{c}$ at $E_{C.M.} = 500$ GeV and $P = 0.9$. Radiative corrections are included.

z_{\pm}^* of Eq. (11). Figs. 1,2 show that, in the LL and RR cases, optimization results in a rather modest increase of sensitivity and of the corresponding discovery limits on Λ_{RR} and Λ_{LL} (by a few percent), since the z^* behavior of the uncertainty is rather flat. Conversely, in the LR and RL cases optimization can substantially increase the sensitivity and the corresponding reachable lower bounds on Λ_{LR} and Λ_{RL} (up to a factor of about 2 for the $c\bar{c}$ case).

5 Bounds on $\Lambda_{\alpha\beta}$ and conclusions

To obtain discovery limits on the four-fermion contact interaction, for each helicity cross section we define a χ^2 (see Eq. (28)):

$$\chi^2 = \left(\frac{\Delta\sigma_{\alpha\beta}}{\delta\sigma_{\alpha\beta}} \right)^2. \quad (36)$$

As a criterion to constrain the allowed values of the contact interaction parameters by the non-observation of the corresponding deviations within the expected uncertainty $\delta\sigma_{\alpha\beta}$, we impose $\chi^2 < \chi_{\text{CL}}^2$, where the actual value of χ_{CL}^2 specifies the desired ‘confidence’ level. The deviations from the SM predictions $\Delta\sigma_{\alpha\beta}$ depend on a single ‘effective’ non-standard parameter, namely, the product of the known relevant SM coupling and contact-interaction coupling in (29). Accordingly, in a χ^2 analysis of data on $\sigma_{\alpha\beta}$, a fit in one effective parameter is involved. Therefore, we take $\chi_{\text{CL}}^2 = 3.84$ for 95% C.L. with a one-parameter fit.

The corresponding discovery reach for the mass scale parameters $\Lambda_{\alpha\beta}$ as a function of luminosity \mathcal{L}_{int} , obtained from the determination of helicity cross sections *via* the measurement of σ_1 and σ_2 at $P = 0.9$ and the optimal z^* with the assumed values of the efficiencies ϵ and of the systematic uncertainties δ^{sys} , is represented by the stars in Figs. 3,4. These figures show that the helicity cross sections $\sigma_{\alpha\beta}$ are quite sensitive to contact interactions, with discovery limits that, at the highest considered luminosity 500 fb $^{-1}$ (and $P = 0.9$), can range from 80 up to 140 times the c.m. energy, depending on the considered final fermion state. Indeed, the best sensitivity is achieved for the $b\bar{b}$ final state, while the worst one

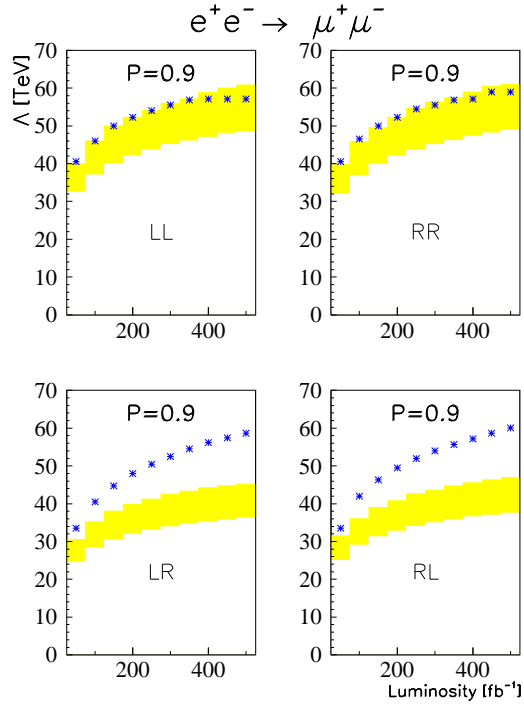


Figure 3: Reach in Λ at 95% C.L., for the process $e^+e^- \rightarrow \mu^+\mu^-$ vs. integrated luminosity. Stars and shaded area indicate, respectively, constraints from helicity cross sections and from the set of observables σ , A_{FB} , A_{LR} and $A_{LR,FB}$.

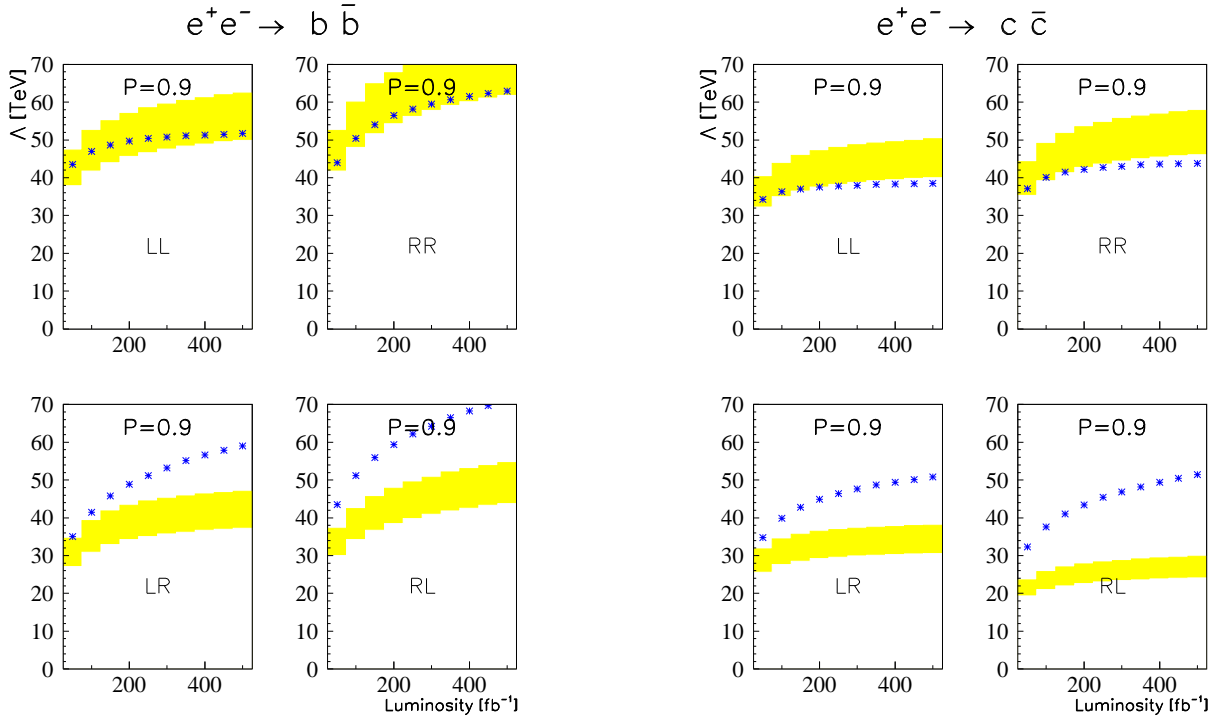


Figure 4: Same as in Fig. 3, but for the processes $e^+e^- \rightarrow b\bar{b}$ and $e^+e^- \rightarrow c\bar{c}$.

corresponds to the $c\bar{c}$ channel. Moreover, we find that decreasing the electron polarization from $P = 1$ to $P = 0.5$ results in a worsening of the sensitivity by 20 – 40%, depending on the final state.

Regarding the role of the assumed uncertainties on the observables under consideration, in the cases of Λ_{LR} and Λ_{RL} the uncertainty turns out to be numerically dominated by the statistical one, especially for the smaller values of the luminosity, and the bounds have less sensitivity to the value of the systematic uncertainty. Conversely, in the cases of Λ_{LL} and Λ_{RR} the results are more dependent on the assumed value of the systematic uncertainty. Asymptotically, for no systematic uncertainty, the bounds on $\Lambda_{\alpha\beta}$ scale like $\mathcal{L}_{\text{int}}^{1/4}$ [10], which would give a factor 1.8 in improvement from 50 to 500 fb⁻¹. Moreover, from Eqs. (5) and (6), a further improvement in the sensitivity to the various Λ -scales in Figs. 3,4 could be obtained if both e^- and e^+ longitudinal polarizations were available [19].⁵ Finally, regarding the role of radiative corrections, one finds that the initial state radiation can lower the search reach by 15–20%.

It is instructive to compare these bounds with those obtained from a χ^2 fit to the set of ‘conventional’ observables $\mathcal{O}_i = \sigma$, A_{FB} , A_{LR} and $A_{LR,\text{FB}}$ quoted in Sect. 2. In this case, the relevant χ^2 can be constructed as follows:

$$\chi^2 = \sum_i \left(\frac{\mathcal{O}_i - \mathcal{O}_i^{\text{SM}}}{\delta \mathcal{O}_i^{\text{SM}}} \right)^2, \quad (37)$$

where the sum is over observables included in the χ^2 , and $\delta \mathcal{O}_i^{\text{SM}}$ is the expected experimental uncertainty on the observable \mathcal{O}_i evaluated, as before, by using the known SM cross sections. Clearly, in contrast to the case of helicity cross sections, the χ^2 of Eq. (37) simultaneously depends on all four contact interaction couplings. Thus, potential cancellations among those, *a priori* free, parameters can occur and lead to either looser, or correlated, bounds on $\Lambda_{\alpha\beta}$. To be quantitative, we may consider the following two representative cases.

The first case represents the simplest situation where all observables \mathcal{O}_i depend on only one contact interaction parameter. This can be realized, *e.g.*, within some specific model. In this case, one can reduce it to a one-parameter fit, but the corresponding bounds on the individual mass scale parameters $\Lambda_{\alpha\beta}$ refer to the specific model. These bounds can be obtained from the χ^2 of Eq. (37) by a procedure analogous to that described above for the helicity cross sections, with $\chi_{\text{CL}}^2 = 3.84$. For that one-parameter case the 95% C.L. bounds on $\Lambda_{\alpha\beta}$ are represented by the upper contours of the shaded regions in Figs. 3,4.

The second case assumes a full four-parameter dependence of the observables. The model-independent analysis including the complete set of four contact interaction couplings as free parameters would identify the observability domain as the region in four-dimensional space external to the surface determined by the equation $\chi^2 = \chi_{\text{CL}}^2$ (where, now, $\chi_{\text{CL}}^2 = 9.49$ corresponds to 95% C.L.). In order to get the bounds on an individual parameter, one should project this surface onto the axis related to that parameter, an analysis that is not simple and, actually, is outside the scope of the present paper. We consider

⁵It seems that a significant positron polarization, of the order of 0.6, might be achievable. We hope to return to a quantitative study, taking into account also e^+ polarization, elsewhere.

here a simplified, but somewhat extreme, case which by construction excludes any accidental cancellation among contributions induced by different parameters. It corresponds to the projection of the above-mentioned surface onto the axis related to one contact parameter, taking all the others at zero value. The corresponding bounds on the individual $\Lambda_{\alpha\beta}$ are represented by the lower contours of the shaded areas in Figs. 3,4. However, in general such contours may be substantially lowered by the potential cancellations, whose effects can spoil the sensitivity to the point that, in some extreme case, a parameter might even remain unconstrained. Therefore, the lower contours in Figs. 3,4 just indicate the maximal potential sensitivity to contact-interaction couplings that can be expected from the model-independent χ^2 analysis of the ‘conventional’ observables in the ideal situation of no cancellation.

The comparison of bounds displayed in Figs. 3,4 from ‘conventional’ observables with those obtained from the analysis using helicity cross sections as basic observables shows that for the LL and RR cases the two kinds of analysis are numerically comparable. Instead, for the LR and RL combinations the sensitivity of helicity cross sections to the relevant contact interaction parameters is appreciably higher. This is mostly due to the optimization through the dependence on the kinematical parameter z^* described in Sect. 3. One should also emphasize that, besides the high sensitivity, helicity cross sections have the qualitative advantage of providing, by definition, unambiguous and fully model-independent information on the new physics parameters of Eq. (2).

Acknowledgements

It is a pleasure to thank Arnd Leike, Sabine Riemann and Luca Trentadue for helpful discussions. This research has been supported by the Research Council of Norway, and by MURST (Italian Ministry of University, Scientific Research and Technology).

References

- [1] E. J. Eichten, K. D. Lane and M. E. Peskin, Phys. Rev. Lett. **50** (1983) 811.
- [2] R. J. Cashmore, et al., Phys. Rept. **122** (1985) 275; R. Rückl, Phys. Lett. **B129** (1983) 363.
- [3] P. Haberl, F. Schrempp, and H.-U. Martyn, in *Physics at HERA*, Proceedings of the workshop, Vol. 2 (1991) p.1133; G. Altarelli, J. Ellis, G. F. Giudice, S. Lola, and M. L. Mangano, Nucl. Phys. **B506** (1997) 3; K. S. Babu, C. Kolda, J. March-Russel, and F. Wilczek, Phys. Lett. **B402** (1997) 367; C. J. C. Burges and H. J. Schnitzer, Phys. Lett. **B134** (1984) 329; K. Cheung, S. Godfrey and J.A. Hewett, in *Proceedings of the 1996 DPF/DPB Summer Study on New Directions for High Energy Physics* (Snowmass 96), Edited by D.G. Cassel, L. Trindle Gennari, R.H. Siemann (SLAC, 1997) p. 989. V. Barger, K. Cheung, K. Hagiwara, and D. Zeppenfeld, Phys. Lett. **B404** (1997) 147; N. Di Bartolomeo and M. Fabbrichesi, Phys. Lett. **B406** (1997) 237; J. Kalinowski, R. Rückl, H. Spiesberger, and P.M. Zerwas, Phys. Lett. **B406** (1997) 314; Z. Phys. **C 74** (1997) 595.

- [4] V. Barger, K. Cheung, K. Hagiwara, and D. Zeppenfeld, Phys. Rev. D **57** (1998) 391; D. Zeppenfeld and K. Cheung, preprint MADPH-98-1081, hep-ph/9810277.
- [5] B. Grzadkowski, Z. Hioki and M. Szafranski, Phys. Rev. D **58** (1998) 035002.
- [6] V. Barger, K. Cheung, D.P. Roy, and D. Zeppenfeld, Phys. Rev. D **57** (1998) 3833.
- [7] P. Osland and A.A. Pankov, Phys. Lett. **B 403** (1997) 93; **B 406** (1997) 328.
- [8] A.A. Babich, A.A. Pankov, and N. Paver, Phys. Lett. **B 426** (1998) 375; **B 452** (1999) 355.
- [9] A.A. Pankov and N. Paver, Phys. Lett. **B 432** (1998) 159.
- [10] B. Schrempp, F. Schrempp, N. Wormes and D. Zeppenfeld, Nucl. Phys. **B296** (1988) 1.
- [11] J.-M. Frère, V.A. Novikov and M.I. Vysotsky, Phys. Lett. **B 386** (1996) 437.
- [12] M. Consoli, W. Hollik and F. Jegerlehner, *in* Z physics at LEP1, ed. G. Altarelli, R. Kleiss and C. Verzegnassi, vol.1, p.7, 1989.
- [13] G. Altarelli, R. Casalbuoni, D. Dominici, F. Feruglio and R. Gatto, Nucl. Phys. **B342** (1990) 15.
- [14] S. Riemann, FORTRAN program ZEFIT Version 4.2; D. Bardin et al., preprint CERN-TH. 6443/92, CERN (1992).
- [15] A. Djouadi, A. Leike, T. Riemann, D. Schaile and C. Verzegnassi, Z. Phys. **C56** (1992) 289.
- [16] Z. Was and S. Jadach, Phys. Rev. **D41** (1990) 1425.
- [17] S. Jadach, J.H. Kühn, R.G. Stuart, Z. Was, Z. Phys. **C38** (1988) 609; Erratum: *ibid* **C45** (1990) 528.
- [18] C. J. S. Damerell and D.J. Jackson, in *Proceedings of the 1996 DPF/DPB Summer Study on New Directions for High Energy Physics* (Snowmass 96), Edited by D.G. Cassel, L. Trindle Gennari, R.H. Siemann (SLAC, 1997) p. 442.
- [19] E. Accomando et al. (ECFA/DESY LC Physics Working Group), Phys. Rept. **299** (1998) 1.